Abstract

Chapter 1

Introduction

1.1 Introduction

Thermal conductivity is one of the important properties in designing a nuclear fuel, since most of the physical phenomenon are thermally governed. In case of high-performance reactors, fuel goes through high fission density at relatively low temperatures. For this reason research reactor fuels are desined for efficient heat rejection. Usually it is composed of assemblies of thin-plates that uses aluminum alloy cladding. This is called 'dispersion' fuels.

The Reduced Enrichment for Research and Test Reactors (RERR) program was initiated in the US in the late 1970s, to develop new fuels. This development of Low-Enriched Uranium (LEU) fuels for high-performance reactors is an important nonproliferatio initiatives [16]. One of the major requirements is having higher Uranium density to offset the decrease in enrichment. Different alloys have been selected and tested. The U-Mo alloy has been identified as a high performance fuel due to its hgih Uranium density and low nuetron capture cross-section [3, 14, 12, 7].

Chapter 2

Methodology

In this work, a Finite Element model is used to solve the steady state heat conduction equation to determinte the effective thermal conductivity of various fuel microstructures. Two types of microstructures were used as simulation domain. Both of the domains contain Xe bubble as fission product. One microstructure (Figure 2.1) contains the Xenon Bubble superlattice sturcture and another microscturcture contains the grain boundary structure (Figure 2.3). The first one represents the intragranular bubble and the second one represents the intergranular bubble. All simulations were performed in 2-D domain. The gas bubble supperlattice structure(GBS) was created based on Miller et al. [9]. According to Miller et al. the bubble size inside the GBS structure follows normal distribution. From these experimental values four diamters were chosen to create FEM model. Since, the GBS inside U-10Mo is FCC, the 2D sturcture was created based on the FCC sturcture. The lattice constant was 12 nm which was also from Miller et al. Lattice constants were kept constants for all four bubble sizes. The bubble sizes were 3.1, 3.6, 3.75 and 4 nm in diameter. The square domains dimension is 80×80 nm, with 91 bubbles inside it with lattice constants of 12. Two dimensional triangulare mesh was used to mesh the domain. Trelis Pro package was used to do the meshing. In the second microsturcture, grain boundary (GB) sturcture is created with Adobe illustrator. The size of the GB structure kept unchanged throughout the drawing. The GB sturcture of U-10Mo was chosen from Miller et al. [10]. This was a SEM (Scanning Electron Microscop image of
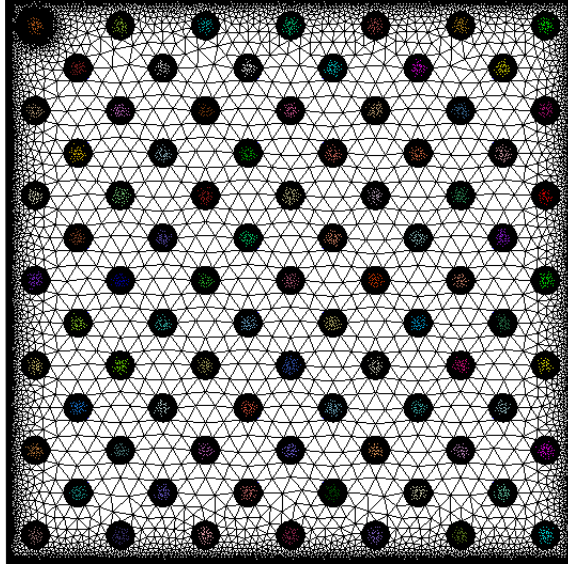
Figure 2.1: Meshed Xenon bubble inside U-10Mo matrix

a FIB (Focused Ion Beam) cross-section showing fission gas bubbles populating in the grain boundaries. This domain was also meshed with triangular mesh. A mesh study was done to chose a meshing size that will optimize the result and the compuational time. The effective thermal conductivity of the domain is determined by applying boundary conditions on each side and solving for temperature field within the domain. In the current work MOOSE Framework [4] was used to obtain the thermal solution.
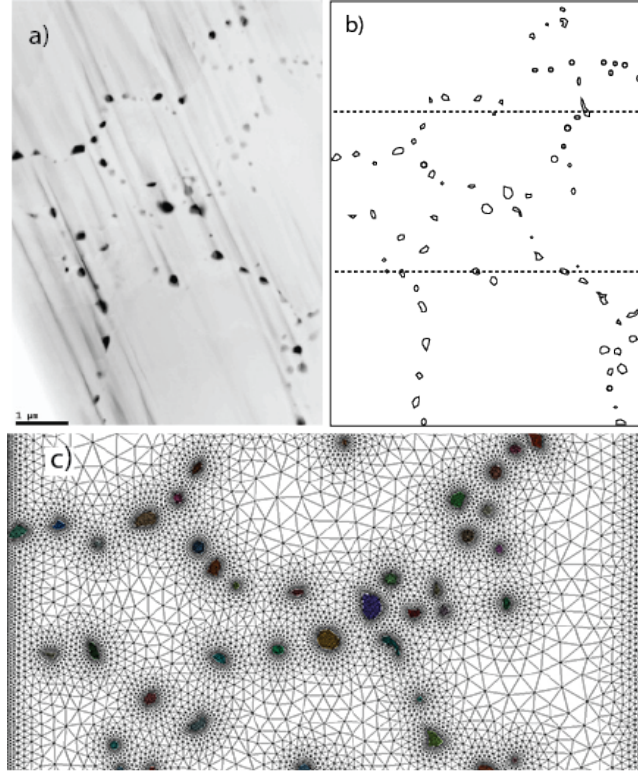
Figure 2.2: a) TEM image of the fission gas bubbles along the grain boundaries from Miller et. al. used for FEM calculations [10] b) Geometry created based on the Grain Boundary fission gas modelling c)FEM mesh with grain boundary fissoin gas

Two material objects were created. Both of these contained the thermal conductivity data for U-10Mo and Xenon. A linear fit of thermal conductivity with respect to temperature was used for U-10Mo which is from Burkes et. al. [1]. Thermal conductivity of Xenon depends both on temperature and pressure [11]. Figure 2.3 shows the change of thermal conductivity with increasing pressure and temperature. Pressure inside the bubble highly depends on the radius and shear modulus of the host material [5, 18]. Xiao et. at. [19] performed atomistic simulation of the small Xenon bubble inside U-MO alloy. According to Xiau et. al. pressure inside the Xenon bubble can go as high as 12 GPa. This increased pressure creates another possibility of having solid Xenon bubbles inside the material [17, 13, 20]. Thermal conductivity data of Xenon above 1000 bar is not available for a wide temeprature range. To evaluate the impact of pressure of Xenon on the overall thermal conductivity, five sets of thermal conductivity data (1bar, 70bar,

220bar, 380bar, 600bar and 1000bar) were used. For each set of data a polynomial fit is used for FEM calculation. The results are discussed in the following section.
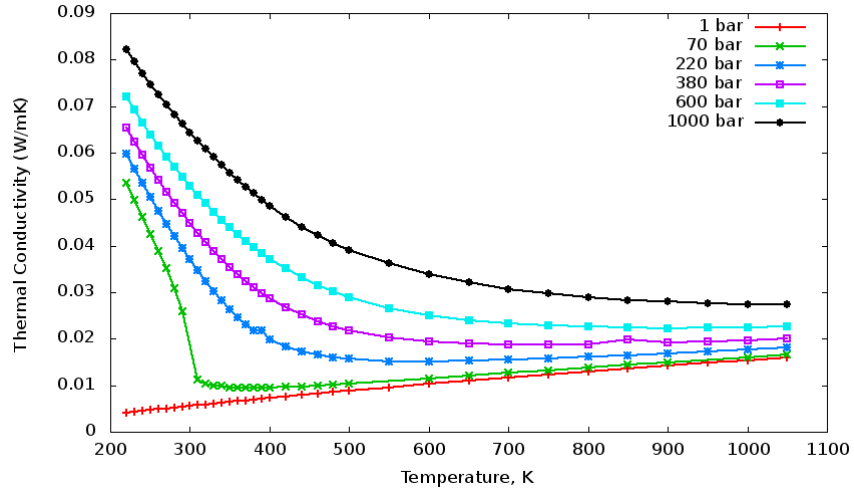

Figure 2.3: Thermal Conductivity of Xenon with increasing pressure from Rabinovich et. al. [11]

Chapter 3

Results

3.1 Results

Figure 3.1 shows the effective thermal conductivity due to Xenon bubble distribution in the intragranular region. Thermal conductivity decreases with the increase in the bubble size. In this simulation thermal conductivity of Xenon was at 1 bar. The FEM result is compared with the theoritical solution for porour material's thermal conductivity, to check whether the FEM results fall in the region. To compare the results the famous Maxwell-Eucken [8] equation was used.

$$\lambda = \lambda_s \frac{\lambda_p + 2\lambda_s + 2\nu_p(\lambda_p - \lambda_s)}{\lambda_p + 2\lambda_s - \nu_p(\lambda_p - \lambda_s)} \tag{3.1}$$

Where, λ = thermal conductivity of the fuel meat

λ_s = thermal conductivity of the continuous phase (U-10Mo)

λ_p = thermal conductivity of the dispersed phase in spherical shape (Xe bubble)

ν_p = volume fraction of the dispersed phase (volume fraction of Xe inside U-10Mo)

Equation 3.1 assumes the pore volume fraction is less than 15% and dispersed uniformly in the solid matrix. The distance between the pores is far enough that they do not interact [2, 15]. The result is also compared with Hashin-Shtrikman upper bound, which is based on a theoritical expression derived for the magnetic permeability of multiphase material [6].

$$\lambda = \frac{1}{4}\left[\lambda_p(3\nu_p - 1) + \lambda_s(2 - 3\nu_p) + \left\{[\lambda_p(3\nu_p - 1) + \lambda_s(2 - 3\nu_p)]^2 + 8\lambda_s\lambda_p\right\}^{\frac{1}{2}}\right]$$

$$(3.2)$$

The compared result is shown in Figure 3.2. As it can be seen from Figure 3.2 that with the increase in temperature there is a slight deviation.
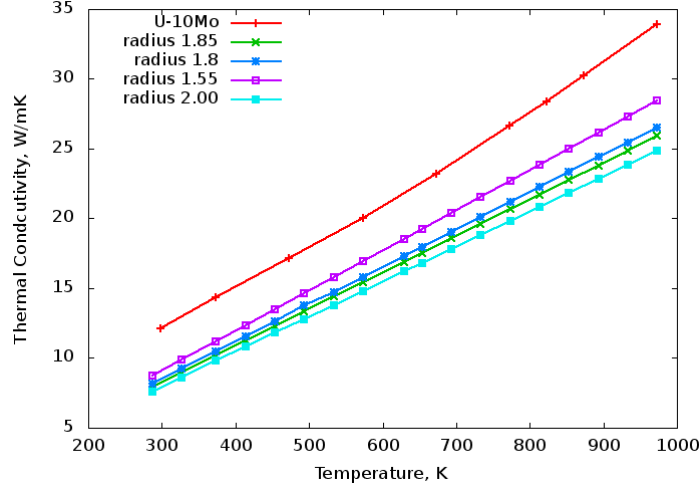

Figure 3.1: Comparison between the thermal conductivity of U-10Mo and the inclusion of Xe bubble of different sizes
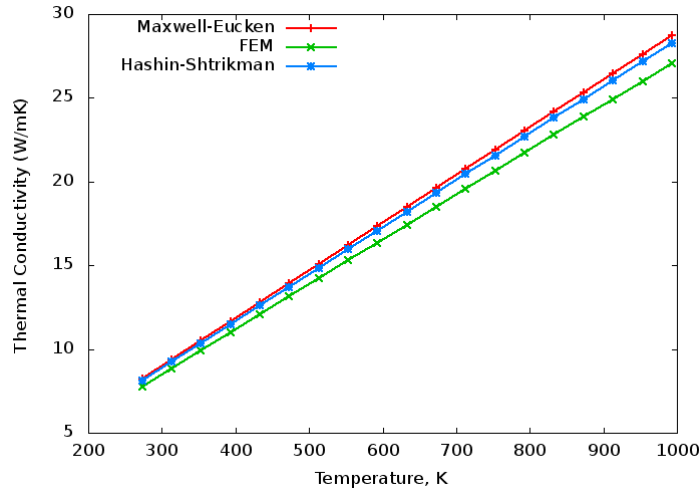

Figure 3.2: Comparison of predicted thermal conductivity of U-10Mo with Xenon bubble against the Maxwell-Eucken and Hashin and Shtrikman

To see tha impact of pressure of Xenon on the overall thermal conductivity, five different pressures were used. Each pressure has a distinctvie thermal conductivity

of Xenon(Figure 2.3). In this study a constant bubble size is used. The result of the simulations is presented in Figure 3.3. The result shows a little to no change on the overall thermal conductivity of the fuel meat. This might be due to the increasing pattern of thermal conductivity with respect to pressure.

To study the grain boundary Xenon bubble, Xenon's thermal conductivity of 1 bar is used. The solution is obtained using Dirichlet boundary condition. The solution is presented in Figure 3.4. With addition of the grain boundary Xenon, overall thermal conductivity drops more than the addition of inragranular bubble.
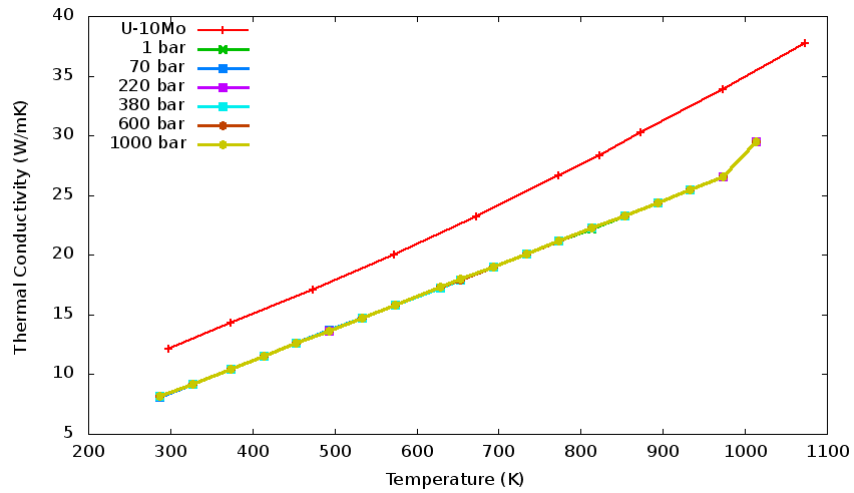

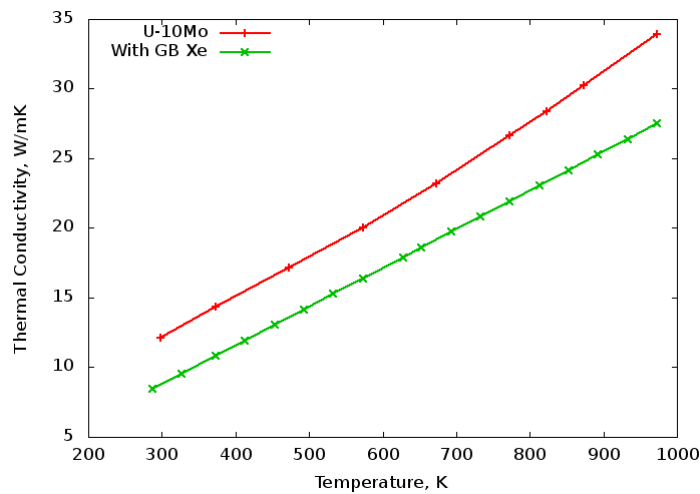Figure 3.3: Over all thermal conductivity U-10Mo using thermal conductivity of Xenon of several pressure

Figure 3.4: Over all thermal conductivity U-10Mo using grain boundary Xenon gas

8

Chapter 4

Discussions and conclusions

Chapter 5

Acknowledgments

Bibliography

[1] Douglas E Burkes et al. "Thermo-physical properties of DU–10wt.% Mo alloys". In: *Journal of Nuclear Materials* 403.1 (2010), pp. 160–166.

[2] CR Clark et al. "Monolithic fuel plate development at Argonne National Laboratory". In: *2003 International Meeting on Reduced Enrichment for Research and Test Reactors, Chicago, IL*. Vol. 1. 10. 2003.

[3] A Ewh et al. "Microstructural Characterization of U-Nb-Zr, U-Mo-Nb, and U-Mo-Ti Alloys via Electron Microscopy". In: *Journal of phase equilibria and diffusion* 31.3 (2010), pp. 216–222.

[4] Derek Gaston et al. "MOOSE: A parallel computational framework for coupled systems of nonlinear equations". In: *Nuclear Engineering and Design* 239.10 (2009), pp. 1768–1778.

[5] GW Greenwood, AJE Foreman, and DE Rimmer. "The role of vacancies and dislocations in the nucleation and growth of gas bubbles in irradiated fissile material". In: *Journal of Nuclear Materials* 1.4 (1959), pp. 305–324.

[6] Zvi Hashin and Shmuel Shtrikman. "A variational approach to the theory of the effective magnetic permeability of multiphase materials". In: *Journal of applied Physics* 33.10 (1962), pp. 3125–3131.

[7] A Landa, P Söderlind, and PEA Turchi. "Density-functional study of bcc U–Mo, Np–Mo, Pu–Mo, and Am–Mo alloys". In: *Journal of Nuclear Materials* 434.1 (2013), pp. 31–37.

[8] James Clerk Maxwell. *A treatise on electricity and magnetism*. Vol. 1. Clarendon press, 1904, p. 440.

[9] BD Miller et al. "Transmission electron microscopy characterization of the fission gas bubble superlattice in irradiated U–7wt% Mo dispersion fuels". In: *Journal of Nuclear Materials* 458 (2015), pp. 115–121.

[10] Brandon D Miller et al. "Advantages and disadvantages of using a focused ion beam to prepare TEM samples from irradiated U–10Mo monolithic nuclear fuel". In: *Journal of Nuclear Materials* 424.1 (2012), pp. 38–42.

[11] Viktor Abramovich Rabinovich et al. "Thermophysical properties of neon, argon, krypton, and xenon". In: (1987).

[12] J Rest, GL Hofman, and Yeon Soo Kim. "Analysis of intergranular fission-gas bubble-size distributions in irradiated uranium–molybdenum alloy fuel". In: *Journal of Nuclear Materials* 385.3 (2009), pp. 563–571.

[13] M Ross and AK McMahan. "Condensed xenon at high pressure". In: *Physical Review B* 21.4 (1980), p. 1658.

[14] DE Smirnova et al. "A ternary EAM interatomic potential for U–Mo alloys with xenon". In: *Modelling and Simulation in Materials Science and Engineering* 21.3 (2013), p. 035011.

[15] David S Smith et al. "Thermal conductivity of porous materials". In: *Journal of Materials Research* 28.17 (2013), pp. 2260–2272.

[16] James L Snelgrove et al. "Development of very-high-density low-enriched-uranium fuels". In: *Nuclear Engineering and Design* 178.1 (1997), pp. 119–126.

[17] LE Thomas. "Condensed-phase xenon and krypton in UO2 spent fuel". In: *Fundamental aspects of inert gases in solids*. Springer, 1991, pp. 431–441.

[18] H Trinkaus. "Energetics and formation kinetics of helium bubbles in metals". In: *Radiation Effects* 78.1-4 (1983), pp. 189–211.

[19] Hongxing Xiao et al. "Atomistic simulations of the small xenon bubble behavior in U–Mo alloy". In: *Materials & Design* 74 (2015), pp. 55–60.

[20] J Zheng et al. "Thermodynamics, compressibility, and phase diagram: Shock compression of supercritical fluid xenon". In: *The Journal of chemical physics* 141.12 (2014), p. 124.

Appendix A

XYZ Algorithm

```
clc
clear all
NN=input('Input the value of N');
%———next 13 lines assign an index IG to each basis function
C=zeros(3,3,3,3);
IG=0;
for I=1:3
    for L=1:NN+1
        for M=1:NN+1
            for N=1:NN+1
             if (L+M+N > NN+3), break, end
            IG=IG+1;
            IC(IG)=1;
            LB(IG)=1;
            MB(IG)=1;
            NB(IG)=1;

            end
        end
    end

end
rank=0.5*(NN+1)*(NN+2)*(NN+3);
NR=IG;
Gamma=zeros(rank,rank);
for IG=1:NR
    for JG=IG:NR
        I=IC(IG);
        J=IC(JG);
        LS=LB(IG)+LB(JG);
        MS=MB(IG)+MB(JG);
        NS=NB(IG)+NB(JG);

        Gamma(IG,JG)=C(I,1,J,1)*LB(IG)*LB(JG)*func(LS-2,MS,NS)+...
```

```
        C( I , 2 , J , 2 )*MB( IG )*MB(JG)* func ( LS ,MS−2,NS )+...
        C( I , 3 , J , 3 )*NB( IG )*NB(JG)* func ( LS ,MS, NS−2 )+...
        C( I , 1 , J , 2 )*LB( IG )*MB(JG )+...
        C( I , 2 , J , 1 )*MB( IG )*LB(JG)* func ( LS−1,MS−1,NS )+...
        C( I , 1 , J , 3 )*LB( IG )*NB(JG )+...
        C( I , 3 , J , 1 )*NB( IG )*LB( IG )* func ( LS−1,MS, NS−1 )+...
        C( I , 2 , J , 3 )*MB(JG)*NB( IG )+...
        C( I , 3 , J , 2 )*NB( IG )*MB(JG)* func ( LS ,MS−1,NS−1 );
    Gamma( JG , IG)=Gamma( IG , JG ) ;
  if ( I==J )  E( IG , IG)=func ( LS ,MS, NS)   ;
     end
end
end


[ vects   v a l s ]= e i g (E\Gamma ) ;
```